Phase Separation and Suppression of the Structural and Magnetic Transitions in Superconducting doped Iron Tellurides, $Fe_{1+x}Te_{1-y}S_y$

P. Zajdel[†], P-Y Hsieh[†‡], E. E. Rodriguez[†], N. P. Butch[⊥], J. D. Magill[⊥], J. Paglione[⊥], P. Zavalij[§], M. R. Suchomel[∥] and M. A. Green[†‡*]

NIST Center for Neutron Research, NIST, 100 Bureau Drive, Gaithersburg. 20878 MD, Departments of Materials Science and Engineering, Center for Nanophysics and Advance Materials and Chemistry, University of Maryland, College Park, MD 20742 and Advanced Photon Source, Argonne National Laboratory, Argonne, IL. 60439

Email: mark.green@nist.gov

Abstract

Single crystal and powder samples of the series of iron chalcogenide superconductors with nominal composition, $Fe_{1.15}Te_{1-y}S_y$, are found to be stable over the range $0 \le y \le 0.15$. They crystallize in the anti-PbO structure that is tetragonal at room temperature and composed of layers of edge-shared $Fe(Te,S)_4$ tetrahedra separated by a van der Waals gap. For $y = 0$, $Fe_{1+x}Te$ ($x \approx 0.12(1)$) is non-superconducting and undergoes a tetragonal (*P4/nmm*) to monoclinic ($P2_1/m$) structural transition at ~ 65 K, associated with the onset of commensurate antiferromagnetic order at **q** = (0.5 0 0.5). We show that on Sulfur substitution, $Fe_{1+x}Te_{1-y}S_y$ becomes orthorhombic (*Pmmn*) at low temperature for $0 \le y \le 0.015$, where the greatly suppressed magnetic scattering is now incommensurate at **q** =

[†] NIST
[∥] APS
[‡] Materials Science and Engineering, University of Maryland
[⊥] Center for Nanophysics and Advance Materials, University of Maryland
[§] Chemistry, University of Maryland

(0.5- δ 0 0.5) and possesses short ranged magnetic correlations that are well fitted with a two-dimensional Warren peak shape. At much higher concentrations of S ($y \geq 0.075$), there is complete suppression of both the low temperature structural transition and magnetic scattering and a superconducting transition at 9 K is observed, although a full resistive transition is not present until $y = 0.15$. Between these two composition regimes, there exists a region of phase separation ($0.025 \leq y \leq 0.05$), where the low temperature powder neutron diffraction data is best refined with a model containing both the tetragonal and orthorhombic phases. Microprobe analysis of a single crystal of composition $Fe_{1.123(5)}Te_{0.948(4)}S_{0.052(4)}$ confirms the presence of compositional variation within the crystals, which explains the observed phase separation.

Introduction

The discovery of superconductivity in $LaO_{1-x}F_xFeAs$ at 26 K[1] marked the onset of establishing a new category of high temperature superconductors based on iron. This ZrCuSiAs-type compound contains alternating layers of PbO-type LaO and the electronically active anti-PbO-type FeAs blocks. It was shown that variation of lanthanide ion greatly affects the superconducting transition temperatures from $CeO_{1-x}F_xFeAs$ (T_C = 41 K)[2], $NdO_{1-x}F_xFeAs$ (T_C = 51 K)[3], $PrO_{1-x}F_xFeAs$ (T_C = 52 K)[4] to $SmO_{1-x}F_xFeAs$ (T_C = 55 K)[5]. Superconductivity in alternative structures was later found in the related $ThCr_2Si_2$-type system, AFe_2As_2 (A=Ba, Sr, Ca)[6,7] and anti-PbFCl structure, AFeAs (A= Na or Li)[8-10]. The same fundamental structural building block in these systems, the FeAs layers, crystallizes without the need of cations in the form of the tetragonal anti-PbO structure, shown in Figure 1, now with doubly charged anions required to maintain

the Fe^{2+} oxidation state, such as in the series Fe(Te, Se S). In this family, FeTe is superconducting with either Se[11] and S[12] inclusion, whereas stoichiometric FeSe[13,14] is superconducting at temperatures as high as 36.7 K under pressure[15,16]. More recently, it has been suggested that $Fe_{1+x}Te$ can support superconductivity at $T_C \approx 13$ K when grown in thin film form[17].

The structural simplicity of Fe(Te, Se, S) systems, along with their propensity to form high quality single crystals, lends this family of superconductors to extensive research on their structure, magnetism and sample homogeneity. One central issue in iron-based superconductivity, which is controlled by both composition and/or pressure, is the competition at low temperature between high (tetragonal) and low (orthorhombic or monoclinic) crystal symmetry; the former is associated with superconductivity, whereas the latter is concomitant with the appearance of a localized moment and no superconductivity[18-23]. The structural phase diagram of the Fe(Te,Se,S) series, is one of the many important differences that distinquishes it from other families of iron-based superconductors. For example, FeSe is superconducting at $T_C \approx 8.5$ K, but is orthorhombic rather than tetragonal at low temperature, yet displays no long ranged magnetic order[13,14,24]. Pressure has a dramatic effect on the superconducting transition temperature[15], increasing it to 36.7 K at 8.9 GPa, as a result of the markedly reduced interlayer separation, before transforming to a non-superconducting NiAs-type structure at higher pressures[16]. $Fe_{1+x}Te$ possesses additional structural complexity as a result of the presence of secondary interstitial Fe ions between the anti-PbO-like blocks. This has important consequences on both its structure and magnetism; $Fe_{1+x}Te$ undergoes a low temperature distortion from tetragonal to monoclinic at $x < 0.12$, which is associated with

the onset of commensurate ($\pi/2$, $\pi/2$) antiferromagnetic order, whereas an orthorhombic symmetry is present at $x > 0.12$, which has incommensurate ($\delta\pi$, $\delta\pi$) antiferromagnetic order[23]. For all compositions the localized moment at $\approx 2\ \mu_B$[23] in the parent compositions is significantly higher than that found in other structural families and with a different propagation vector that is rotated by 45° compared with other structural families, giving a unique double stripe feature[19-22,25]. A comprehensive study of the $Fe_{1+y}Te_{1-x}S_x$ demonstrated the importance of stoichiometry in these compounds and correlation between magnetism and superconductivity that warrants a detailed structural study[26].

Here we show that on S doping, the commensurate antiferromagnetic and monoclinic structure of $Fe_{1+x}Te$ first becomes orthorhombic, with incommensurate short ranged two-dimensional antiferromagnetic correlations, before complete suppression of both the magnetic and structural transitions leads to a tetragonal superconductor at $T_C \sim 9$ K. Compositional variation within the samples accounts for a phase separated region between the orthorhombic and tetragonal regimes. Increasing the amount of sulfur dopant on the Te sites also reduced the amount of interstitial iron, therefore the observed changes in the magnetism is likely a result of both of these factors. These results further stress the uniqueness of the Fe(Te, Se, S) phase diagram compared with the other iron based superconductors, although the observed superconducting transition temperature and tetrahedral bond variance is consistant with all families of iron-based superconductors.

Experimental Details

Powder samples of $Fe_{1+x}Te_{1-y}S_y$ ($0 < y < 0.15$) were synthesized by direct reaction of Fe, Te and S in an evacuated sealed quartz tubes. All materials were heated for 2 days at 400

°C to initially react all of the Te, followed by heating at 700 °C for 2 days to form the tetragonal anti-PbO phase. Starting compositions had a fixed nominal Fe content of x = 0.15 excess, which proved to be optimal in the formation of single phase material free from $FeTe_2$ and the hexagonal FeTe impurities. Iron loss occurs during the thermal treatment and final iron compositions were determined by a combination of single crystal X-ray diffraction, powder neutron diffraction and microprobe analysis. Samples with higher sulfur content (y > 0.15) showed inclusion of FeS as an impurity and lattice parameters comparable to the x = 0.15 composition, demonstrating the end of the solid solution under these synthesis conditions, as shown in Figure S1.

Single crystals for X-ray diffraction were silver – black plates of approximate dimension 0.01 × 0.2 × 0.2 mm^3. Data were collected at 250 (2) K on a three-circle diffractometer system equipped with Bruker Smart Apex II CCD area detector using a graphite monochromator and a Mo K_α fine-focus sealed tube (λ= 0.71073 Å). The detector was placed at a distance of 5.2 cm from the crystal. Powder neutron diffraction was performed on the BT1 high resolution difractometer at the NIST Center for Neutron research. Data were collected using the Ge (311) monochromator at λ = 2.0782 Å and the Cu (311) monochromator at λ = 1.5401 Å, with an in-pile collimation of 15'. Rietveld refinement was performed using the GSAS[27] and Fullprof[28] packages. Chemical composition analysis was performed using a JEOL JXA-8900 Electron Microprobe in wavelength-dispersive spectrometry (WDS) mode. The electron accelerating voltage was 20 kV providing beam of around 10 μm in diameter. Synchrotron X-ray powder diffraction was performed at the 11-BM beam line at the Advance Photon Source, Argonne at a wavelength of λ = 0.458737 Å.

Results

Single Crystals of $Fe_{1+x}Te_{1-y}S_y$ Single crystal X-ray diffraction of a crystal with nominal composition $Fe_{1.15}Te_{0.95}S_{0.05}$ was refined at 250 (2) K in the P4/nmm tetragonal symmetry, yielding an actual stoichiometry of $Fe_{1.123(5)}Te_{0.948(4)}S_{0.052(4)}$. The structure of the anti-PbO structure is given in Figure 1 (a). Although within experimental error the Te : S ratio is exactly the starting composition, the amount of interstial iron is lower than expected, which has been previously reported[23]. One of the most significant features of the sulfur doped iron telluride structure is the significant shifting of the sulfur position from the Te site. Figure 1 (b) shows a detailed layout of the Fe tetrahedon. The majority ion, Te, lies at a position at ≈ 2.61 Å from Fe at the center of the tetrahedron and at an angle of ≈ 43º from the (*a b* 0.5) plane, while S is significantly closer to Fe at ≈ 2.26 Å and at only ≈ 43º from Fe plane. These values are entirely consistent with the values obtain for the pure phase of FeS (mackinawite), which shows a Fe – S bond distance of 2.231Å[29], and the pure anti-PbO structure of FeTe that gives an identical bond distance of around 2.6 Å[30]. This type of position splitting results from the very large difference in the ionic radii of the two anions and has previously been observed in Fe(Te,Se)[31]. To further eludidate the exact distribution of anions, a maximum entropy refinement was performed on powder neutron diffraction data obtained at 4 K from a powder sample of the same composition. This data formed a series of experiments that is discussed in full later in the paper. Neutron diffraction was used as its nuclear scattering gives a clearer distribution of density. The reconstruction of the nuclear scattering density of the combined (Te, S) site is shown in Figure 2 (b) (ii) and confirms the very distinct positions of the two anions.

This shifting of the S sites gives a Te – S separation of around 0.5 Å and its variation with composition is discussed later.

Magnetic Structure of $Fe_{1+x}Te_{1-y}S_y$ Low temperature powder neutron diffraction experiments performed at 4 K, confirmed a dramatic change in the magnetism as a function of sulfur doping. Figure 2(a) shows the principal magnetic reflection, located to the left of the nuclear (001) reflection at around 19º two-theta, for several compositions of $Fe_{1+y}Te_{1-x}S_x$. For x = 0, the commensurate magnetic reflection occurs at propagation vector, **q** = (0.5 0 0.5) and the structure was refined in the monoclinic $P2_1/m$ space group, consistent with previous measurements[23]. The refined composition of $Fe_{1.122(6)}Te$ represents the upper limit of the commensurate monoclinic $Fe_{1+x}Te$ phases, compositions with greater interstitial Fe content are susceptible to incommensurate antiferromagnetic order that is associated with an orthorhombic structure of *Pmmn* symmetry[23]. The inclusion of small amounts of S in $Fe_{1+x}Te_{1-y}S_y$ (y = 0.0075, 0.015 and 0.025) shows an immediate alteration of the magnetic ground state; all of these phases are now incommensurate despite the decreased amount of interstitial Fe due to the increased S content. The opposite trend has been observed in the $Fe_{1+x}Te$ phases, where decreasing the amount of interstitial Fe tends to stabilize the commensurate antiferromagnetic structure.

Another interesting effect on the magnetic properties with S doping was found by analyzing the peak profile shape of the magnetic reflections. The intensity of the magnetic reflection at **q** = (0.5-δ 0 0.5) decreases, while the peak width increases. Such short range incommensurate magnetic scattering was previously been observed for the

$Fe_{1+x}Te_{1-y}Se_y$ system[23]. The asymmetric peak profile shape of this magnetic scattering is indicative of two-dimensional correlations. Therefore these reflections were fitted with a Warren peak shape function[32] that allows for the direct extraction of magnetic correlation length. Figure 2(b) and 2(c) shows how the magnetic propagation vector, intensity and correlation length varies as a function of S doping. For $y \geq 0.05$ in $Fe_{1+x}Te_{1-y}S_y$, the magnetic scattering was either not present or too broad to measure, indicative of a very rapid suppression of the magnetic scattering as a function sulfur doping (≈ 5 %).

Structure and Stoichiometry of $Fe_{1+x}Te_{1-y}S_y$ The apparent difference in the interstitial iron inclusion from the nominal stoichiometry that was observed with single crystal X-ray diffraction was further evaluated as a function of y in $Fe_{1+x}Te_{1-y}S_y$ by Rietveld refinement of the structure with powder neutron diffraction data. Figure 2(d) shows the observed amount of interstitial iron on the secondary Fe site as a function of S doping. As found for $Fe_{1+x}(Te,Se)$[33], there is a correlation such that the amount of interstitial iron decreases with increases substitution of Te with the smaller anion.

Structural refinements using the powder neutron diffraction data at 4 K, shows that within the incommensurate magnetic regime of $Fe_{1+x}Te_{1-y}S_y$ ($0.0075 \leq y \leq 0.025$), the crystal structure is orthorhombic with the *Pmmn* space group; the same space group employed in the incommensurate phases of $Fe_{1+x}Te$ with $x > 0.12$. At much higher concentrations of S ($y \geq 0.05$), the best single phase fit occurs in the tetragonal *P4/nmm* space group present at high temperature, implying the absence of a low temperature distortion with higher S doping. However the quality of the fits at 4 K for composition of $Fe_{1+x}Te_{1-y}S_y$ between $0.025 \leq y \leq 0.05$ were noticeably worse and gave higher goodness-

of-fit factors. Further Rietveld refinements employing a two-phase model that included both an orthorhombic *Pmmn* phase and a tetragonal *P4/nmm* phase, gave markedly improved fits to the data. A summary of the structural phase diagram showing the lattice parameters as a function of composition for $Fe_{1+x}Te_{1-y}S_y$ at 4 K is given in Figure 3, outlining the transformation from monoclinic, to orthorhombic, to a phase-separated regime before the tetragonal phase is stable over all temperatures. The inset to Figure 3 shows the phase fraction of the tetragonal and orthorhombic structures as a function of sulfur doping. The structural parameters obtained from Rietveld refinements of powder neutron diffraction data at 4 K is given in Table 1. The inclusion of the S makes remarkeable little difference to the bond lengths and angles despite the changes in structural symmetry and magnetism. Figure 4 (a) shows the three key iron bond distances, Fe – Fe2, Fe – Te and Fe – S, as a function of composition. For all compositions the Fe – Te and Fe – S remain flat around 2.6 and 2.21 Å, respectively as observed in the single crystal study. The Fe – Fe2 does get significantly longer with higher sulfur composition, this reflects a shifting of the intestitial iron further out of the Te plane and closer to the adjacent Fe – (Te,S) layer. The bond angles of Te – Fe – Te are highly distorted from the ideal tetrahedron value of 109.47º at around 117º and 95º, and are largely unaffected by S composition, see figure 4 (b). The difference in length between the Te and S sites, or Te – S separation, shown in Figure 4 (c), is constant at just over 0.5 Å for the tetragonal section of the phase diagram. There is some indication that this separation increases on reducing S content, but the reducing sensitivity with such low concentrations of S limits any definitive conclusions.

To further elucidate the origin of the phase separation a series of high-resolution synchrotron X-ray powder diffraction experiments were performed, as well as a microprobe analysis of a single crystal of nominal composition $Fe_{1.15}Te_{0.95}S_{0.05}$. Figure 5(a) shows a comparison of the peak width of the (001) reflection of $Fe_{1+x}Te_{1-y}S_y$ (y = 0.1, 0.125 and 0.15) compared with a LaB_6 NIST 660a standard at ambient temperature, confirming that there is considerable sample broadening that was not apparent in the neutron powder diffraction data. Such broadening commonly occurs when there is a distribution of compositions on a microscopic level that is averaged in a diffraction experiment. To explore how this distribution manifested itself within a single crystal, microprobe analysis measurements were performed at 39 positions across a single crystal previously determined by single crystal X-ray diffraction to be of composition, $Fe_{1.123(5)}Te_{0.948(4)}S_{0.052(4)}$. An *xy* map of the determined compositions is given in Figure 5(b) and demonstrates a continuous variation of the amount of S present within the samples from one end of the crystal to the other.

Superconductivity A series of resistivity measurements was performed to evalute the superconducting properties of the $Fe_{1+x}Te_{1-y}S_y$ series. A comparison is shown in Figure 6 between $Fe_{1+x}Te_{0.85}S_{0.15}$ and $Fe_{1+x}Te_{0.875}S_{0.125}$, which shows that the former is a bulk superconductivity at $T_c \approx 9$ K, whereas the latter does not show a full resistive transiton. The filamentary origin of superconductivity has been previously discussed for certain ranges of composition for this and other systems in the Fe(Te,Se,S) series[26,33].

Discussion

The substitution of Te (ionic radii = 2.21 Å) for the smaller S (ionic radii = 1.84 Å) ion, predictably reduces both lattice parameters and volume. However, the higher S content also has the effect of reducing the amount of interstitial Fe, which further promotes the contracting volume trend, until no interstitial iron is observed for y = 0.15. In the study by Hu et al on $Fe_{1+x}Te_{1-y}S_y$, a similar reduction of the institial iron was observed[26]. It is interesting to note that the optimal superconductivity in $Fe_{1+x}Te_{1-y}S_y$ at $y \approx 0.15$, arises in the samples without interstitial iron, which has previously been observed for the selenide series, $Fe_{1+x}Te_{1-y}Se_y$[33]. First principal calcultions have predicted that the large localized moment observed on this site in $Fe_{1+x}Te$ is likely to have a detrimental effect on the superconductivity[34,35]. However, it is unclear whether the role of the S substitution is to apply chemical pressure on the system by contracting the lattice and thereby promoting superconductivity, or whether it simply suppresses the inclusion of interstitial Fe ions and stabilizes a stoichiometric and superconducting material. A similar question was answered in the $Fe_{1+x}Se$ system, where it was found that superconductivity was destroyed at $x > 0.01$[36].

The Shannon and Prewitt ionic radii for six-coordinated Te^{2-}, Se^{2-} and S^{2-} are 2.21 Å, 1.98 Å and 1.84 Å, respectively[37]. The extensive difference between these anions can explain the inhomogeneity within the crystals and the tendency to form Te and S rich regions, which ultimately leads to the phase separation at low temperature in $Fe_{1+}Te_{1-y}S_y$, when y is near the tetragonal – orthorhombic compositon boundary and some of the sample undergoes a structural phase transition while another part remains tetragonal. The

extent of the phase separation is expected to be greater and more detectable in the sulphur-doped systems than the analogous Se compounds due to greater size difference.

Optimal superconductivity in $Fe_{1+}Te_{1-y}Se_y$ occus at $x \approx 0.5$[33], which gives an average anion size of ≈ 2.095 Å, which is very similar to the average anion radius (2.1545 Å) achieved with the 15% doping of the much smaller S ion in $Fe_{1.0}Te_{0.85}S_{0.15}$, implying that structural considerations are important in understanding the optimal superconducting samples. Another property of the chalcogen anion to consider is that of its electronegativity. While Pauling electronegativities of S and Se are quite similar (2.58 and 2.55, respectively), the Te value of 2.1 is much lower and closer to the value for Fe(II) of 1.83[38]. An obvious consequence is that the interaction between Fe and Te is expected to be more covalent that that between Fe and Se/S. Nevertheless, since the electronegativites in S and Se are similar, differences in the optimal superconducting doping levels can be attributed to differences in the anion size alone. Since Hu et al did not take diffraction data on $Fe_{1+}Te_{1-y}S_y$ below 80 K, they did not report the magnetic and structural phase separation. However, their resistivity measurements do show a coexistance of magnetic ordering and superconductivity for $y = 0.03$[26], consistent with our phase diagram.

For both $Fe_{1+x}Te$ and $Fe_{1+x}Te_{1-y}S_y$ systems, the incommensurate magnetic structure possess orthorhombic nuclear symmetry and the non-magnetic compositions possess tetragonal symmetry, further highlighting the direct correlation between the magnetism and lattice degrees of freedom across different groups of Fe-based superconductors. As the spin density wave and superconductivity compete with the same Fermi surface, it has been proposed that there should be little coexistence of the two states.[39] Therefore, the

coexistence of phases to result from chemical inhomogeneity within the sample, rather than the intrinsic nature of the electronic structure, corroborates this prediction. Coexistence of superconductivity and magnetism, which occurs in some phase diagrams but not others, has been widely discussed, although the highest superconducting transition temperatures are always found in compositions with no long ranged magnetic order[26,40-46]. However, in the case of $Fe_{1+x}Te_{1-y}S_y$ this co-existence is unquestionably the result of an inhomogeneous distribution of anions.

Conclusion

In summary, $Fe_{1+x}Te_{1-y}S_y$ is an example of the Fe(Te,Se,S) family of superconductors that distinguish themselves from other iron based superconductors in numerous ways. We show that that on sulfur inclusion, the magnetism of monoclinic $Fe_{1+x}Te$ transforms through an orthorhombic phase with two-dimensional incommensurate short ranged magnetic scattering to a superconducting tetragonal phase, with optimal superconductivity occurring at $Fe_{1.0}Te_{0.85}S_{0.15}$. The composition variation within the sample was such that, for compositions around the orthorhombic – tetragonal boundary, phase separation occurs at low temperature. Furthermore, the superconducting transition temperature of 9 K for $FeTe_{0.85}S_{0.15}$ is consistent with the variation of transition temperature with bond variance (a measure of the extent of the tetrahedral distortion from the ideal 109.47º (see Figure S2), as previous noted[22]. In addition to their similar average anion radii, $Fe_{1+x}Te_{1-y}Se_y$ and $Fe_{1+x}Te_{1-y}S_y$ both show optimal superconductivity at compositions with little or no excess iron, the control of which will be essential in understanding the relative importance of these factors.

Reference

(1) Kamihara, Y.; Watanabe, T.; Hirano, M.; Hosono, H. *Journal of the American Chemical Society* **2008**, *130*, 3296.

(2) Chen, G. F.; Li, Z.; Wu, D.; Li, G.; Hu, W. Z.; Dong, J.; Zheng, P.; Luo, J. L.; Wang, N. L. *Physical Review Letters* **2008**, *100*.

(3) Ren, Z. A.; Yang, J.; Lu, W.; Yi, W.; Shen, X. L.; Li, Z. C.; Che, G. C.; Dong, X. L.; Sun, L. L.; Zhou, F.; Zhao, Z. X. *Epl* **2008**, *82*.

(4) Ren, Z. A.; Yang, J.; Lu, W.; Yi, W.; Che, G. C.; Dong, X. L.; Sun, L. L.; Zhao, Z. X. *Materials Research Innovations* **2008**, *12*, 105-106.

(5) Ren, Z. A.; Lu, W.; Yang, J.; Yi, W.; Shen, X. L.; Li, Z. C.; Che, G. C.; Dong, X. L.; Sun, L. L.; Zhou, F.; Zhao, Z. X. *Chinese Physics Letters* **2008**, *25*, 2215-2216.

(6) Rotter, M.; Tegel, M.; Johrendt, D. *Physical Review Letters* **2008**, *101*.

(7) Chen, G. F.; Li, Z.; Li, G.; Hu, W. Z.; Dong, J.; Zhou, J.; Zhang, X. D.; Zheng, P.; Wang, N. L.; Luo, J. L. *Chinese Physics Letters* **2008**, *25*, 3403-3405.

(8) Pitcher, M. J.; Parker, D. R.; Adamson, P.; Herkelrath, S. J. C.; Boothroyd, A. T.; Ibberson, R. M.; Brunelli, M.; Clarke, S. J. *Chemical Communications* **2008**, 5918-5920.

(9) Wang, X. C.; Liu, Q. Q.; Lv, Y. X.; Gao, W. B.; Yang, L. X.; Yu, R. C.; Li, F. Y.; Jin, C. Q. *Solid State Communications* **2008**, *148*, 538-540.

(10) Parker, D.; Vavilov, M.; Chubukov, A.; Mazin, I. *Physical Review B* **2009**, *80*, 100508.

(11) Yeh, K. W.; Huang, T. W.; Huang, Y. L.; Chen, T. K.; Hsu, F. C.; Wu, P. M.; Lee, Y. C.; Chu, Y. Y.; Chen, C. L.; Luo, J. Y.; Yan, D. C.; Wu, M. K. *Epl* **2008**, *84*.

(12) Mizuguchi, Y.; Tomioka, F.; Tsuda, S.; Yamaguchi, T.; Takano, Y. *Applied Physics Letters* **2009**, *94*, 012503.

(13) Hsu, F.; Luo, J.; Yeh, K.; Chen, T.; Huang, T.; Wu, P.; Lee, Y.; Huang, Y.; Chu, Y.; Yan, D.; Wu, M. *PNAS* **2008**, *105*, 14262-14264.

(14) McQueen, T. M.; Huang, Q.; Ksenofontov, V.; Felser, C.; Xu, Q.; Zandbergen, H.; Hor, Y. S.; Allred, J.; Williams, A. J.; Qu, D.; Checkelsky, J.; Ong, N. P.; Cava, R. J. *Physical Review B* **2009**, *79*.

(15) Mizuguchi, Y.; Tomioka, F.; Tsuda, S.; Yamaguchi, T.; Takano, Y. *Applied Physics Letters* **2008**, *93*, 152505.

(16) Medvedev, S.; Mcqueen, T. M.; Troyan, I. A.; Palasyuk, T.; Eremets, M. I.; Cava, R. J.; Naghavi, S.; Casper, F.; Ksenofontov, V.; Wortmann, G.; Felser, C. *Nature Materials* **2009**, *8*, 630.

(17) Han, Y.; Li, W. Y.; Cao, L. X.; Wang, X. Y.; Xu, B.; Zhao, B. R.; Guo, Y. Q.; Yang, J. L. *Physical Review Letters* **2010**, *104*, 017003.

(18) de la Cruz, C.; Huang, Q.; Lynn, J. W.; Li, J. Y.; Ratcliff, W.; Zarestky, J. L.; Mook, H. A.; Chen, G. F.; Luo, J. L.; Wang, N. L.; Dai, P. C. *Nature* **2008**, *453*, 899-902.

(19) Zhao, J.; Huang, Q.; de la Cruz, C.; Li, S. L.; Lynn, J. W.; Chen, Y.; Green, M. A.; Chen, G. F.; Li, G.; Li, Z.; Luo, J. L.; Wang, N. L.; Dai, P. C. *Nature Materials* **2008**, *7*, 953-959.

(20) Qiu, Y.; Bao, W.; Huang, Q.; Yildirim, T.; Simmons, J. M.; Green, M. A.; Lynn, J. W.; Gasparovic, Y. C.; Li, J.; Wu, T.; Wu, G.; Chen, X. H. *Physical Review Letters* **2008**, *101*.

(21) Huang, Q.; Qiu, Y.; Bao, W.; Green, M. A.; Lynn, J. W.; Gasparovic, Y. C.; Wu, T.; Wu, G.; Chen, X. H. *Physical Review Letters* **2008**, *101*.

(22) Kreyssig, A.; Green, M. A.; Lee, Y.; Samolyuk, G. D.; Zajdel, P.; Lynn, J. W.; Bud'ko, S. L.; Torikachvili, M. S.; Ni, N.; Nandi, S.; Leao, J. B.; Poulton, S. J.; Argyriou, D. N.; Harmon, B. N.; McQueeney, R. J.; Canfield, P. C.; Goldman, A. I. *Physical Review B* **2008**, *78*.

(23) Bao, W.; Qiu, Y.; Huang, Q.; Green, M. A.; Zajdel, P.; Fitzsimmons, M. R.; Zhernenkov, M.; Chang, S.; Fang, M.; Qian, B.; Vehstedt, E. K.; Yang, J.; Pham, H. M.; Spinu, L.; Mao, Z. Q. *Phys. Rev. Lett.* **2009**, *102*, 247001.

(24) Margadonna, S.; Takabayashi, Y.; McDonald, M. T.; Kasperkiewicz, K.; Mizuguchi, Y.; Takano, Y.; Fitch, A. N.; Suard, E.; Prassides, K. *Chemical Communications* **2008**, 5607-5609.

(25) Qiu, Y.; Kofu, M.; Bao, W.; Lee, S.; Huang, Q.; Yildirim, T.; Copley, J.; Lynn, J.; Wu, T.; Wu, G.; Chen, X. In *Physical Review B* 2008; Vol. 78.

(26) Hu, R.; Bozin, E. S.; Warren, J. B.; Petrovic, C. *Physical Review B* **2009**, *80*, 214514.

(27) Larson, A. C.; Von Dreele, R. B.; Los Alamos National Laboratory Report LAUR 86-748: 1994.

(28) Rodriguez-Carvajal, J. In *Physica B* 1993; Vol. 192, p 55.

(29) Berner, R. A. *Science* **1962**, *137*, 669.

(30) Haraldsen, H.; Groenvol, F.; Vihovde, J. *Tidsskrift for Kjemi og Bergvesen* **1944**, *4*, 96.

(31) Tegel, M.; Lohnert, C.; Johrendt, D. *Solid State Communications* **2010**, *150*, 383.

(32) Warren, B. In *Physical Review* 1941; Vol. 59, p 693.

(33) Sales, B. C.; Sefat, A. S.; McGuire, M. A.; Jin, R. Y.; Mandrus, D.; Mozharivskyj, Y. *Physical Review B* **2009**, *79*, 094521.

(34) Han, M. J.; Savrasov, S. Y. *Phys. Rev. Lett.* **2009**, *103*, 067001.

(35) Zhang, L. J.; Singh, D. J.; Du, M. H. *Physical Review B* **2009**, *79*.

(36) McQueen, T.; Huang, Q.; Ksenofontov, V.; Felser, C.; Xu, Q.; Zandbergen, H.; Hor, Y.; Allred, J.; Williams, A.; Qu, D.; Checkelsky, J.; Ong, N.; Cava, R. In *Physical Review B* 2009; Vol. 79.

(37) Shannon, R. D. *Acta Cryst A.* **1976**, *32*, 751.

(38) Pauling, L. *The Nature of the Chemical Bond*; Cornell University, Ithaca, NY, 1960.

(39) Singh, D. J.; Du, M.-H.; Zhang, L.; Subedi, A.; An, J. *Physica C* **2009**, *469*, 886.

(40) Drew, A. J.; Pratt, F. L.; Lancaster, T.; Blundell, S. J.; Baker, P. J.; Liu, R. H.; Wu, G.; Chen, X. H.; Watanabe, I.; Malik, V. K.; Dubroka, A.; Kim, K. W.; Rossle, M.; Bernhard, C. *Physical Review Letters* **2008**, *101*.

(41) Bernhard, C.; Drew, A. J.; Schulz, L.; Malik, V. K.; Roessle, M.; Niedermayer, C.; Wolf, T.; Varma, G. D.; Mu, G.; Wen, H.-H.; Liu, H.; Wu, G.; Chen, X. H. *New Journal of Physics* **2009**, *11*, 055050.

(42) Laplace, Y.; Bobroff, J.; Rullier-Albenque, F.; Colson, D.; Forget, A. *Physical Review B* **2009**, *80*, 140501.

(43) Park, J.; Inosov, D.; Niedermayer, C.; Sun, G.; Haug, D.; Christensen, N.; Dinnebier, R.; Boris, A.; Drew, A.; Schulz, L.; Shapoval, T.; Wolff, U.; Neu, V.; Yang, X.; Lin, C.; Keimer, B.; Hinkov, V. *Phys. Rev. Lett.* **2009**, *102*, 117006.

(44) Khasanov, R.; Bendele, M.; Amato, A.; Babkevich, P.; Boothroyd, A.; Cervellino, A.; Conder, K.; Gvasaliya, S.; Keller, H.; Klauss, H.-H.; Luetkens, H.; Pomjakushin, V.; Pomjakushina, E.; Roessli, B. *Physical Review B* **2009**, *80*, 140511.

(45) Ryan, D. H.; Cadogan, J. M.; Ritter, C.; Canepa, F.; Palenzona, A.; Putti, M. *Physical Review B* **2009**, *80*, 220503.

(46) Zhang, Y.; Wei, J.; Ou, H.; Zhao, J.; Zhou, B.; Chen, F.; Xu, M.; He, C.; Wu, G.; Chen, H.; Arita, M.; Shimada, K.; Namatame, H.; Taniguchi, M.; Chen, X.; Feng, D. *Phys. Rev. Lett.* **2009**, *102*, 127003.

(47) Azuah, R. T.; Kneller, L. R.; Qui, Y.; Tregenna-Piggott, P. L. W.; Brown, C. M.; Copley, J. R. D.; Dimeo, R. M. *J. Res. Natl. Inst. Stan. Technol.* **2009**, *114*, 341.

Figure and Table Caption

Figure 1 (a) The anti-PbO-type structure of $Fe_{1-x}Te$, composed of layers of tetragonal Fe(1) (orange) – Te (yellow) units lying in the xy plane, separated along the z axis by partially occupied Fe(2) interstitial sites. Suphur doping occurs on the Tellurium sites. (b) The structure of $Fe_{1.123(5)}Te_{0.948(4)}S_{0.052(4)}$ as determined by single crystal X-ray diffraction.

Figure 2 (a) Section of the powder neutron diffraction data for nominal compositions, $Fe_{1.15}Te$, $Fe_{1.15}Te_{0.9925}S_{0.0075}$, $Fe_{1.15}Te_{0.9985}S_{0.015}$ and $Fe_{1.15}Te_{0.9975}S_{0.025}$ (top to bottom), showing a large reduction in ordered moment on S inclusion in the $Fe_{1.15}Te$ lattice leading a transition from a commensurate **q** = (0.5 0 0.5) propagation vector to an incommensurate one. The pattern for $Fe_{1+x}Te$ is from Rietveld refinement analysis, whereas the broad asymmetry magnetic scattering for S doped compounds are fitted to a Warren peak shape, implying the magnetism exhibits short ranged two-dimensional correlation. (b) Variation of the magnetic propagation vector as a function of sulfur doping. (c) Variation of the magnetic intensity and magnetic correlation length as a function of sulfur doping. (d) Variation of interstitial Fe ions as a function of sulfur doping, as determined by Rietveld refinement of powder neutron diffraction data

Figure 3 Lattice parameters of the $Fe_{1+x}Te_{1-y}S_y$ series at 4 K, showing the evolution from the orthorhombic *Pmmn* symmetry (*a* dark blue, *c* dark green). Phase separated compositions, where the neutron powder diffraction data was best fitted with a two-phase model, lies between $0.025 \leq x \leq 0.075$, before the appearance of the superconducting tetragonal *P4/nmm* phase (*a* light blue, *c* light green). Solubility limit was $x \sim 0.15$ under these synthesis conditions.

Figure 4 (a) Iron bond distances, (b) Fe – (Te,S) bond angles and (c) separation in the S and Te anion positionsin the $Fe_{1+x}Te_{1-y}S_y$ series, obtained from fitting the powder neutron diffraction pattern at 4 K.

Figure 5 (a) Comparision of the (001) peak width in $Fe_{1+x}Te_{1-y}S_y$ with a LB6 660a standard, demonstrating significant sample broadening. (b) Composition variation of a single crystal with nominal formula, $Fe_{1+x}Te_{0.95}S_{0.05}$ as determined by xy mapping using energy dispersive spectroscopy. A total of 39 positions spread evenly over the crystal were measured to generate the map using the DAVE software[47].

Figure 6 A comparison of the resistivity of $Fe_{1+x}Te_{0.875}S_{0.125}$ and $Fe_{1+x}Te_{0.85}S_{0.15}$ showing a full resistive transition is only found at the end of the solid solution.

Table 1 Structural parameters from Rietveld refinement of powder neutron diffraction data all collected at 4 K. The orthorhombic atomic positions are Fe (0.75 0.25 z), Te (0.25 0.25 z), interstitial Fe2 (0.25 0.25 z) and S (0.25 0.25 z). The tetragonal phase possess atomic positions of Fe (0.75 0.25 0.5), Te (0.25 0.25 z), interstitial Fe2 (0.25 0.25 z) and S (0.25 0.25 z). [1] The crystallographic information for the sulfur position in $Fe_{1+x}Te_{0.9925}S_{0.0075}$ has large error bars due to the very low occupancy. [2] The atomic positions of the minor phase in $Fe_{1+x}Te_{0.975}S_{0.025}$ and $Fe_{1+x}Te_{0.95}S_{0.05}$ were fixed to the values obtained in the majority phase of the neighboring composition, due to instability resulting from such low phase fraction.

Figure 1 (a)

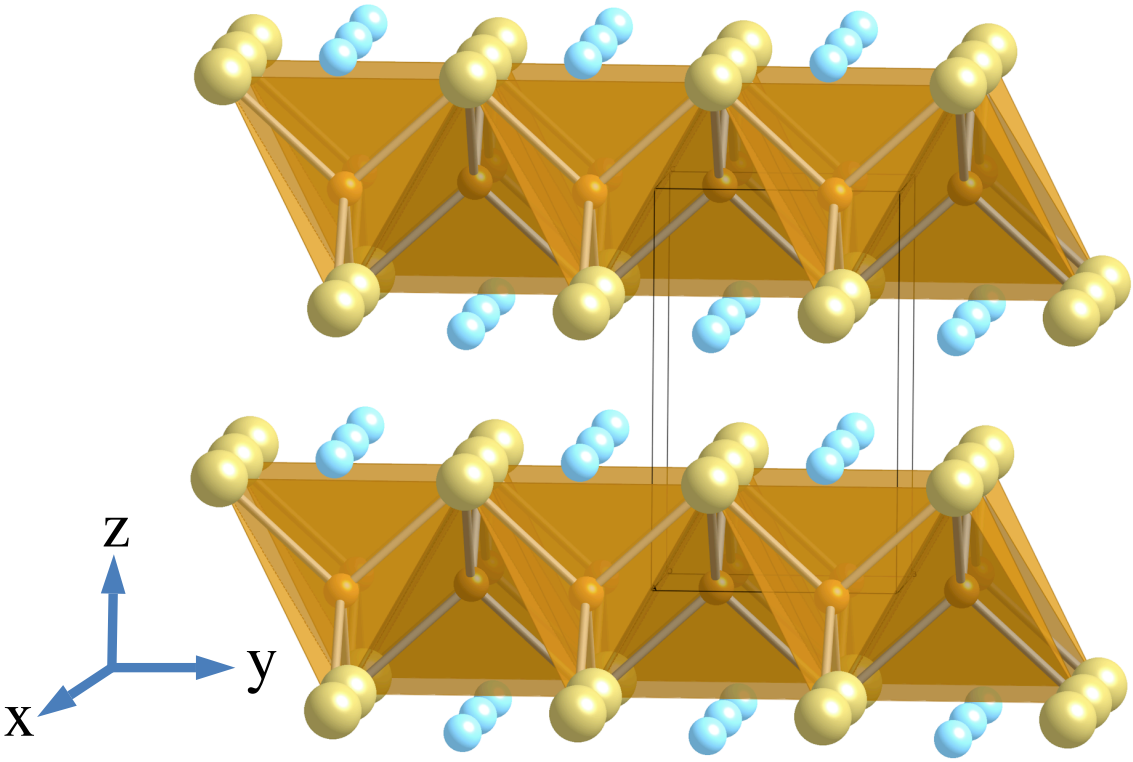

Figure 1 (b)

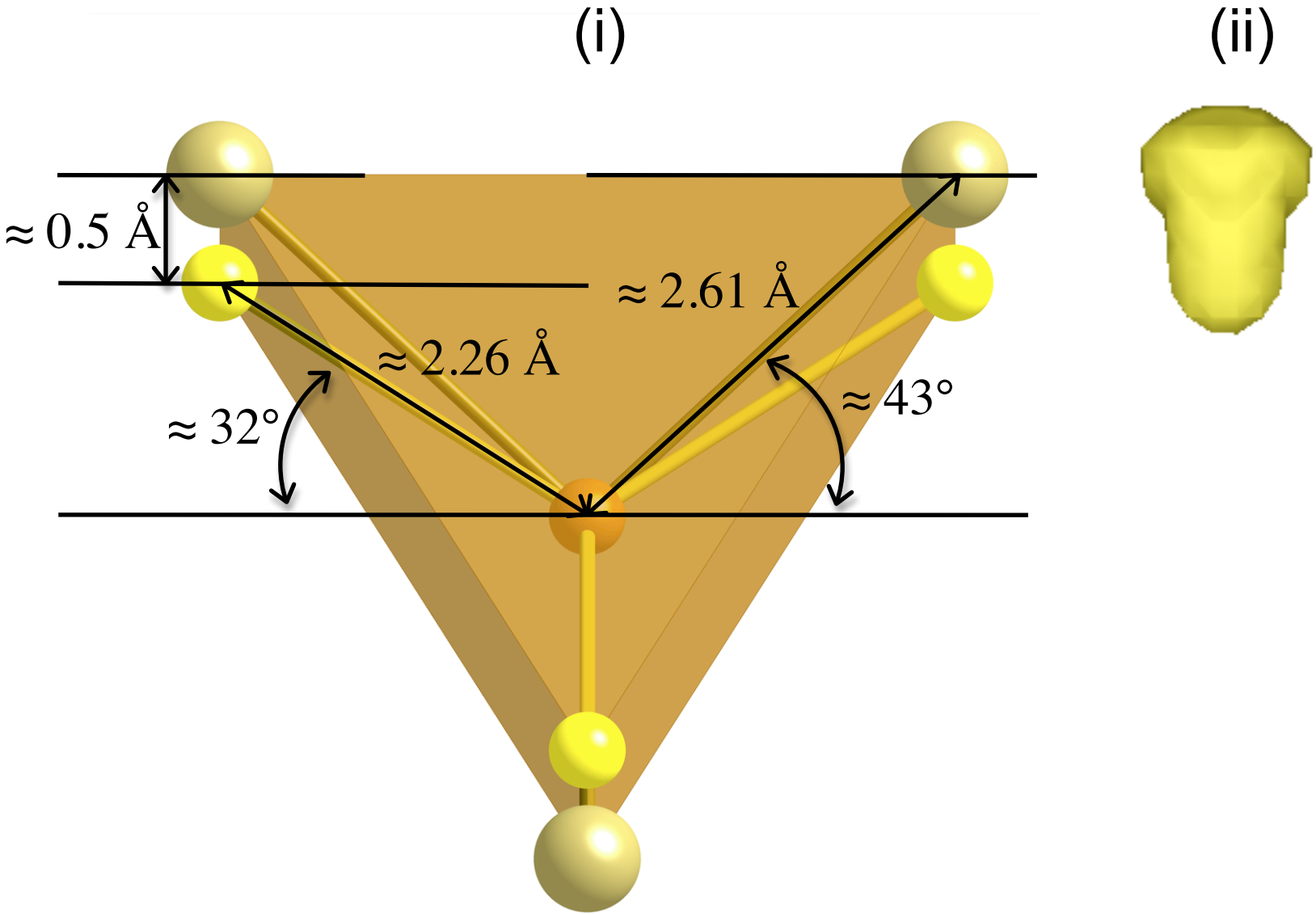

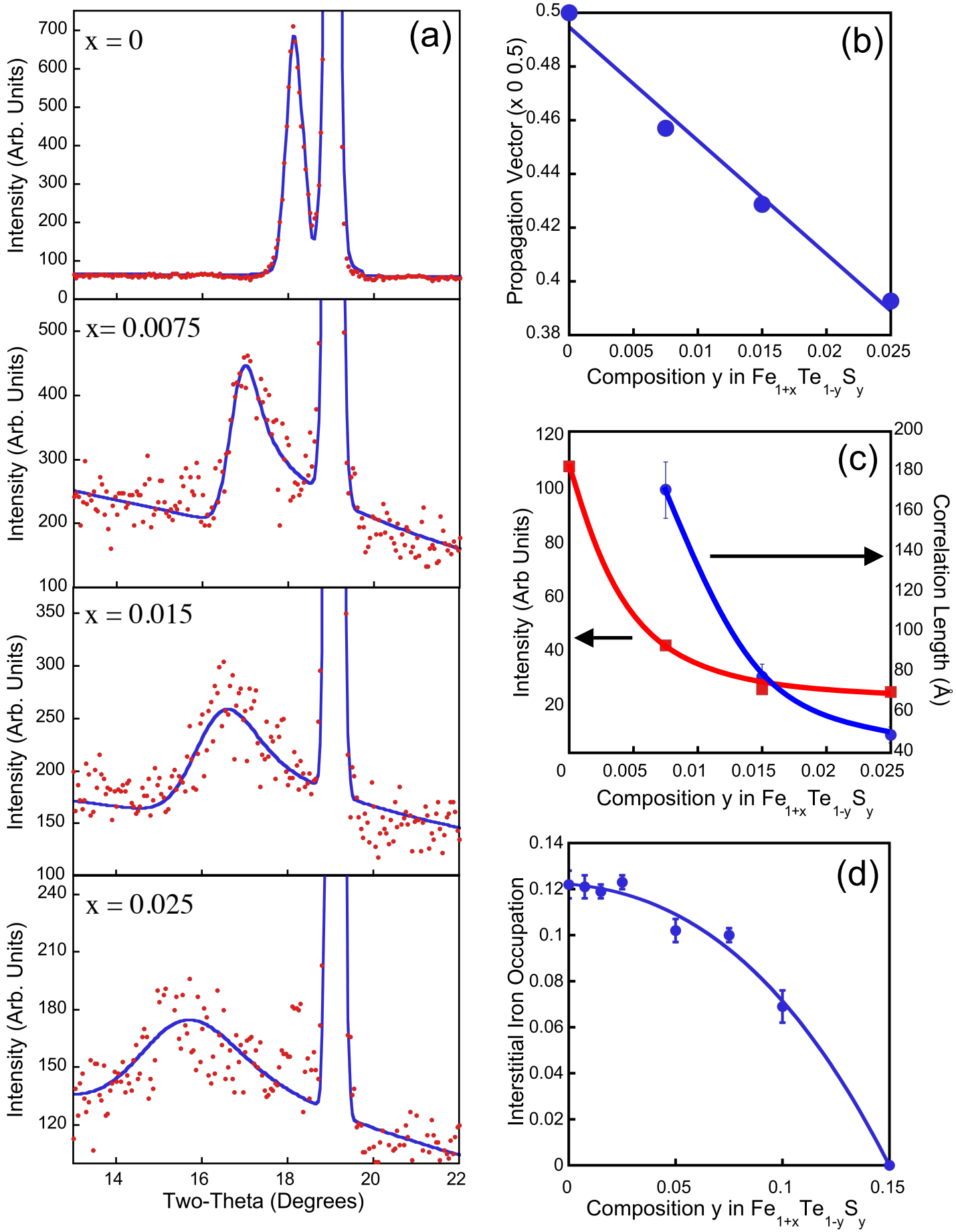
(a)
x = 0
x= 0.0075
x = 0.015
x = 0.025
Intensity (Arb. Units)
Two-Theta (Degrees)
(b)
Propagation Vector (x 0 0.5)
Composition y in Fe1+xTe1-ySy
(c)
Intensity (Arb Units)
Correlation Length (Å)
Composition y in Fe1+xTe1-ySy
(d)
Interstitial Iron Occupation
Composition y in Fe1+xTe1-ySy

Figure 2

Figure 3

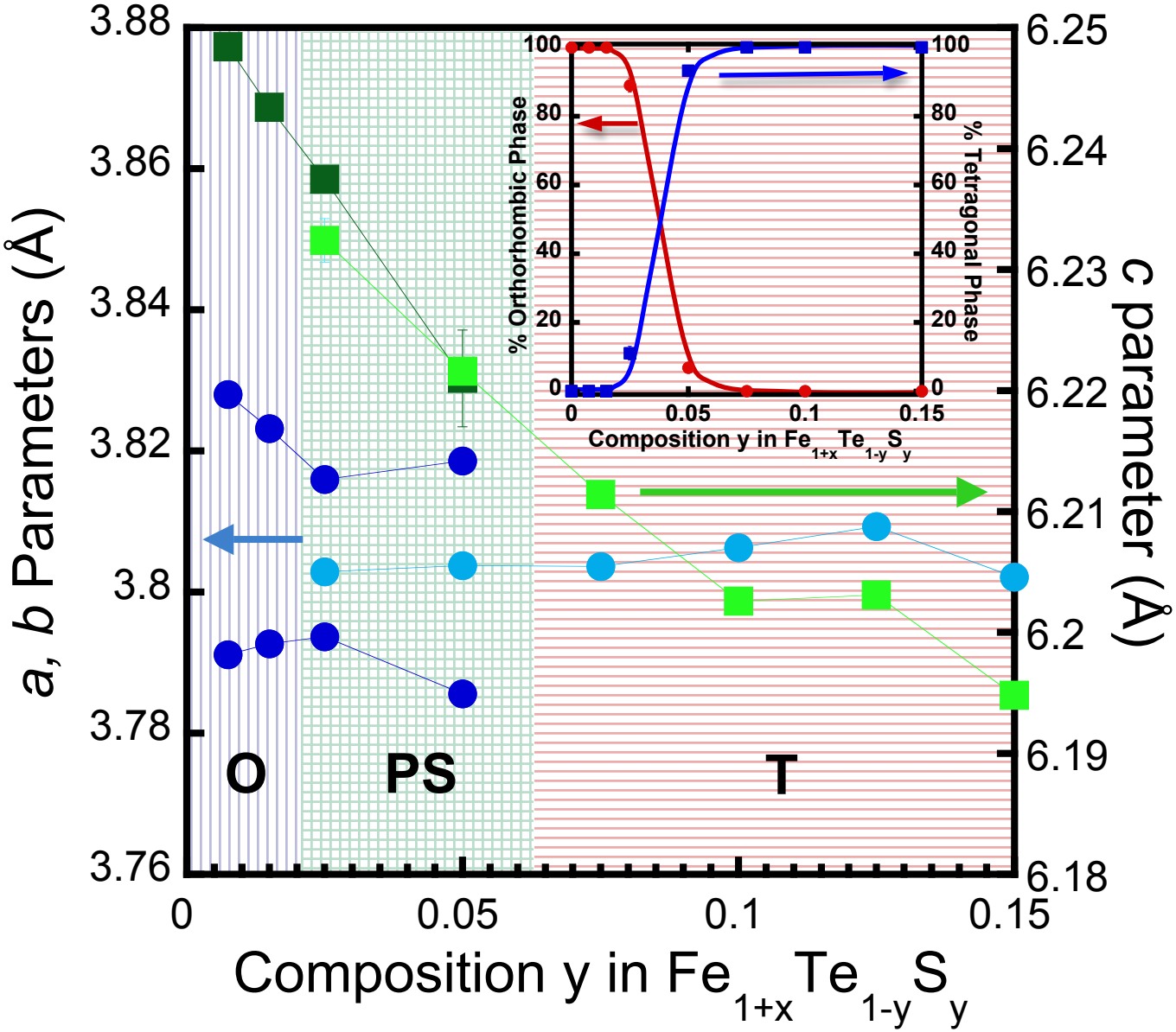
3.88
3.86
3.84
3.82
3.8
3.78
3.76
a, b Parameters (Å)
6.25
6.24
6.23
6.22
6.21
6.2
6.19
6.18
c parameter (Å)
0
0.05
0.1
0.15
Composition y in Fe1+x Te1-y Sy
O
PS
T
% Orthorhombic Phase
% Tetragonal Phase
100
80
60
40
20
0
0
0.05
0.1
0.15
Composition y in Fe1+x Te1-y Sy

Figure 4

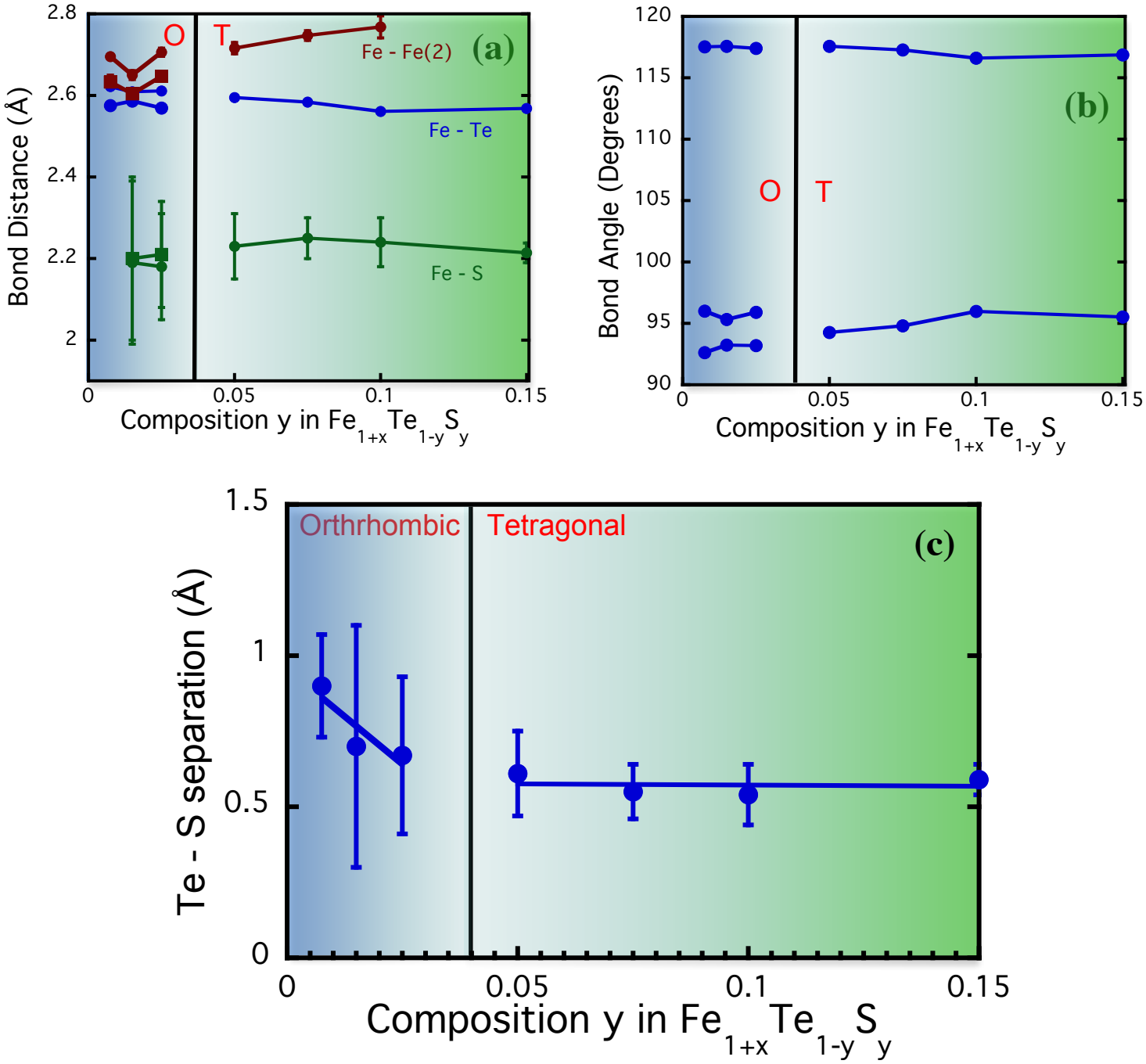
Bond Distance (Å)
2.8
2.6
2.4
2.2
2
O
T
Fe - Fe(2)
(a)
Fe - Te
Fe - S
0
0.05
0.1
0.15
Composition y in Fe1+xTe1-ySy
Bond Angle (Degrees)
120
115
110
105
100
95
90
O
T
(b)
Composition y in Fe1+xTe1-ySy
Te - S separation (Å)
1.5
1
0.5
0
Orthrhombic
Tetragonal
(c)
Composition y in Fe1+xTe1-ySy

Parameter	$Fe_{1+x}Te_{0.9925}S_{0.0075}$	$Fe_{1+x}Te_{0.985}S_{0.015}$	$Fe_{1+x}Te_{0.975}S_{0.025}$		$Fe_{1+x}Te_{0.95}S_{0.05}$		$Fe_{1+x}Te_{0.925}S_{0.075}$	$Fe_{1+x}Te_{0.9}S_{0.1}$	$Fe_{1+x}Te_{0.985}S_{0.15}$
Crystal System	Orthorhombic	Orthorhombic	Orthorhombic	Tetragonal	Orthorhombic	Tetragonal	Tetragonal	Tetragonal	Tetragonal
Propagation Vector	(0.4570 (3) 0 0.5)	(0.4286 (3) 0 0.5)	(0.3926 (2) 0 0.5)	-	-	-	-	-	-
Symmetry	P m m n	P m m n	P m m n	P 4/n m m	P m m n	P 4/n m m	P 4/n m m	P 4/n m m	P 4/n m m
a (Å)	3.8280 (2)	3.8232 (1)	3.8163 (1)	3.8029 (5)	3.8186 (14)	3.80378 (9)	3.8036 (1)	3.80629 (24)	3.80215 (15)
b (Å)	3.7912 (2)	3.7927 (1)	3.7940 (1)		3.7856 (12)				
c (Å)	6.2484 (3)	6.2434 (2)	6.2378 (2)	6.2324 (18)	6.221 (4)	6.22159 (18)	6.2114 (2)	6.2026 (5)	6.19481 (28)
Volume ($Å^3$)	90.680 (8)	90.531 (5)	90.317 (4)	90.135 (32)	89.93 (7)	90.018 (4)	89.863 (4)	89.863 (11)	89.554 (6)
Fe (z)	0.4930 (7)	0.4959 (5)	0.4942 (6)	[2]	[2]				
Te (z)	0.2172 (11)	0.2170 (5)	0.2181 (5)	[2]	[2]	0.2163 (5)	0.2184 (5)	0.2236 (11)	0.2214 (8)
Fe2 (z)	0.7995 (39)	0.7902 (25)	0.8017 (22)	[2]	[2]	0.8117 (32)	0.8190 (27)	0.824(6)	0.8409 (23)
S (z)	0.37 (27)[1]	0.33 (6)	0.32 (4)	[2]	[2]	0.314 (23)	0.306 (14)	0.311 (18)	0.317 (8)
Fe2 Occupancy	0.121 (5)	0.119 (3)	0.123 (3)	[2]	[2]	0.102 (5)	0.100 (3)	0.069 (7)	_
Phase Fraction (%)	100	100	89 (2)	11 (2)	6.8 (8)	93.2 (8)	100	100	100

Table 1

Figure 5

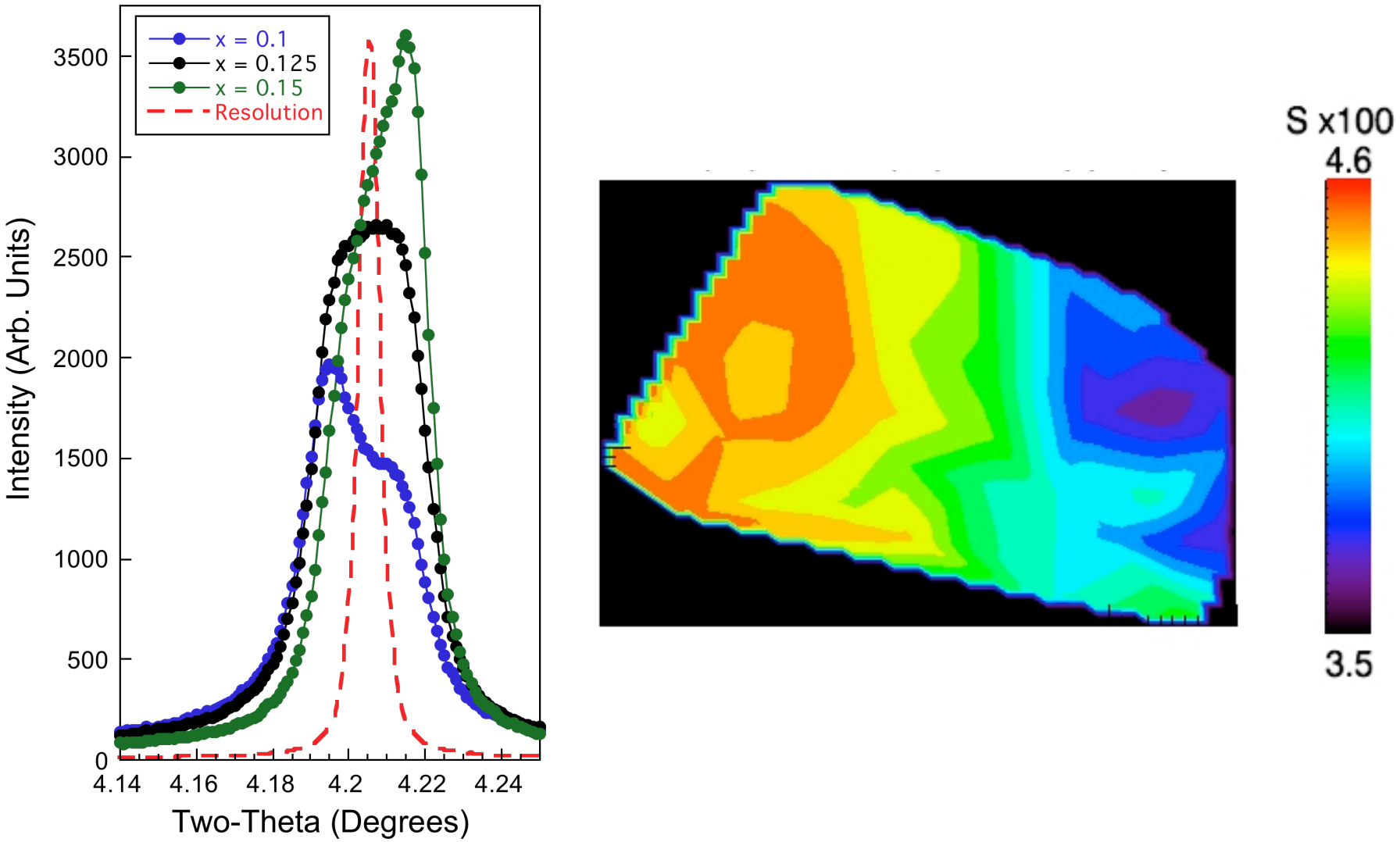
x = 0.1
x = 0.125
x = 0.15
Resolution
Intensity (Arb. Units)
3500
3000
2500
2000
1500
1000
500
0
4.14
4.16
4.18
4.2
4.22
4.24
Two-Theta (Degrees)
S x100
4.6
3.5

Figure 6

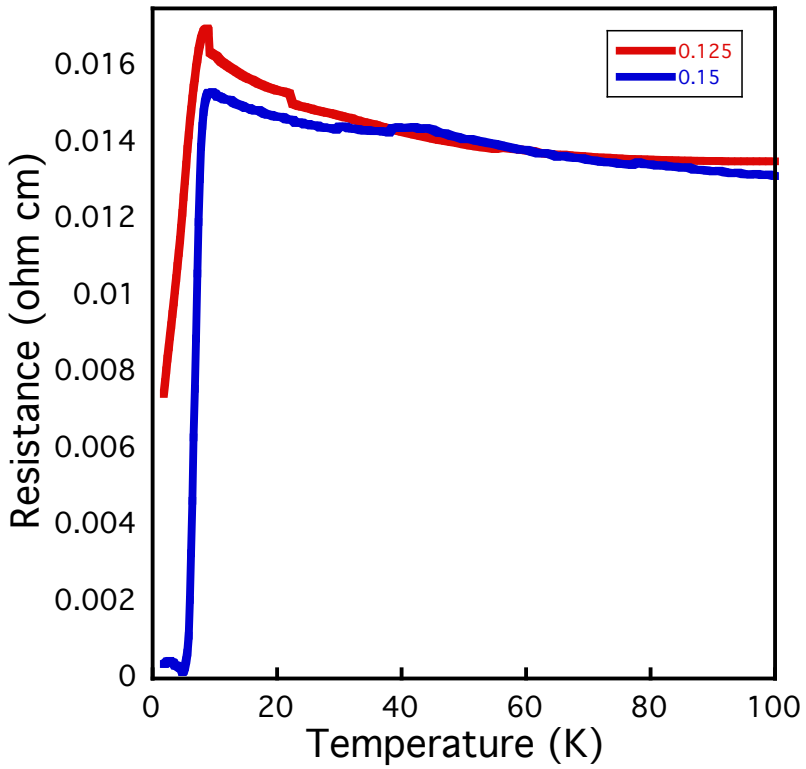
0.125
0.15
Resistance (ohm cm)
0.016
0.014
0.012
0.01
0.008
0.006
0.004
0.002
0
0
20
40
60
80
100
Temperature (K)

Supplementary Information

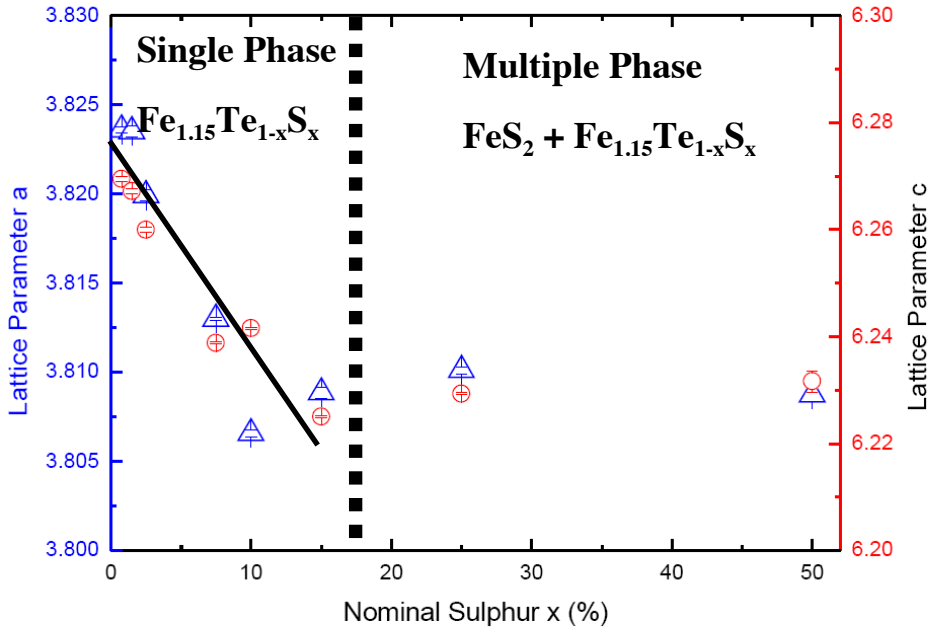

Figure S1 Lattice parameters as determined by powder X-ray diffraction showing adherence to Vegard's law for single phase compositions up to 15%. Composition with higher sulfur content show unit cells similar to that determined for $Fe_{1.15}Te_{0.85}S_{0.15}$ with additional sulfur containing impurities, as a result of the end of the solid solution under these ambient pressure conditions.

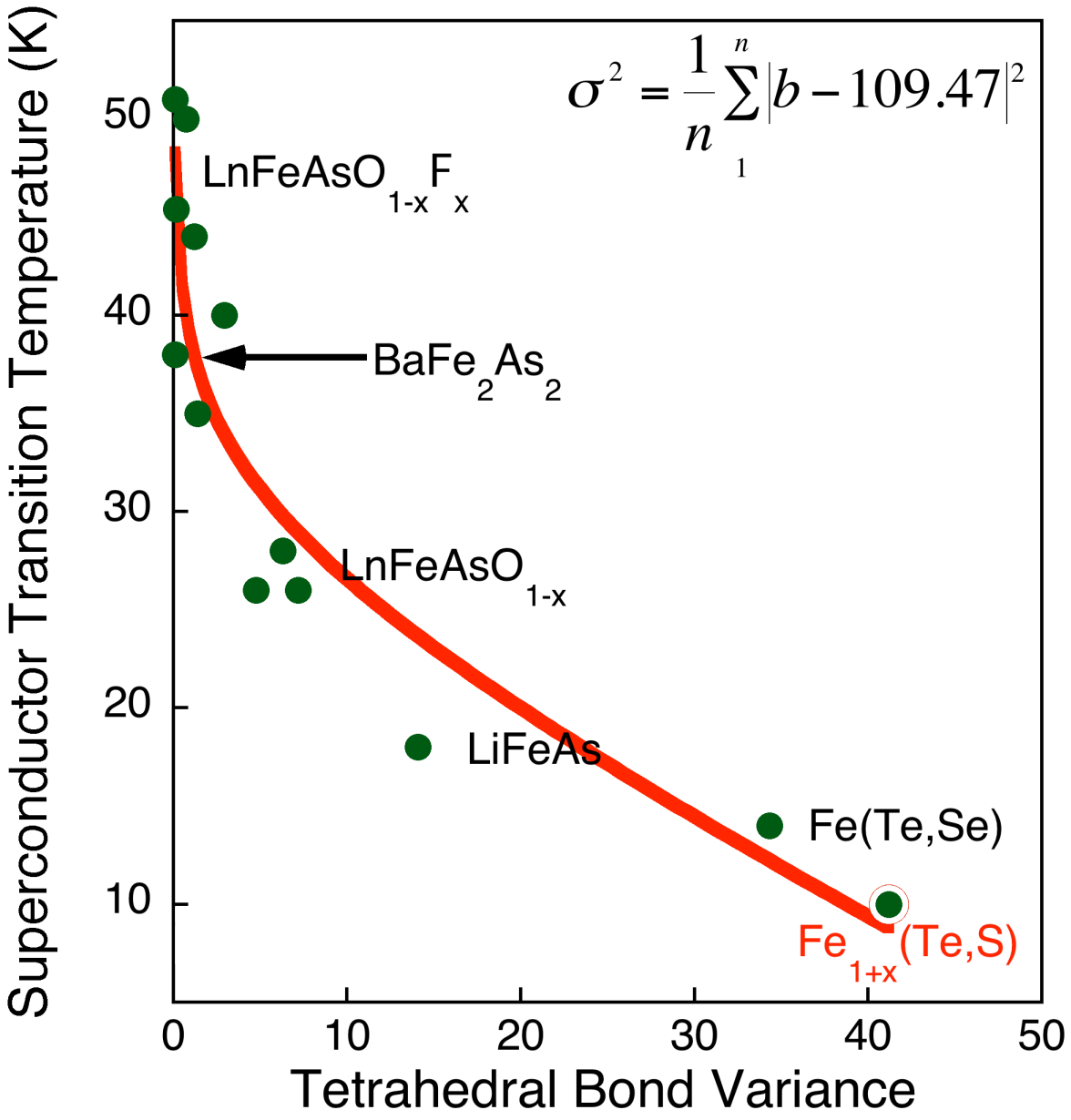

Figure S2 Tetrahedral bond angle variance for various families of Fe-based superconductors, demonstrating the dependence of the superconducting transition temperature with distortion of the six X – Fe – X bond angles. The new Fe_{1+x}(Te, S) shows consistency with those previously reported.